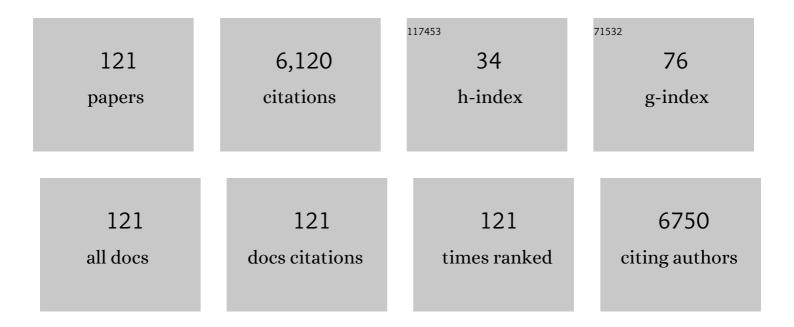
Yasushi Yamaguchi

List of Publications by Year in descending order

Source: https://exaly.com/author-pdf/3618561/publications.pdf Version: 2024-02-01



#	Article	IF	CITATIONS
1	Land use and land cover change in Greater Dhaka, Bangladesh: Using remote sensing to promote sustainable urbanization. Applied Geography, 2009, 29, 390-401.	1.7	798
2	Overview of Advanced Spaceborne Thermal Emission and Reflection Radiometer (ASTER). IEEE Transactions on Geoscience and Remote Sensing, 1998, 36, 1062-1071.	2.7	687
3	Analysis of urban heat-island effect using ASTER and ETM+ Data: Separation of anthropogenic heat discharge and natural heat radiation from sensible heat flux. Remote Sensing of Environment, 2005, 99, 44-54.	4.6	286
4	Global correlation analysis for NDVI and climatic variables and NDVI trends: 1982-1990. International Journal of Remote Sensing, 2002, 23, 3873-3878.	1.3	285
5	Using remote sensing and GIS to detect and monitor land use and land cover change in Dhaka Metropolitan of Bangladesh during 1960–2005. Environmental Monitoring and Assessment, 2009, 150, 237-49.	1.3	273
6	The global distribution of pure anorthosite on the Moon. Nature, 2009, 461, 236-240.	13.7	265
7	Global monitoring of interannual changes in vegetation activities using NDVI and its relationships to temperature and precipitation. International Journal of Remote Sensing, 2001, 22, 1377-1382.	1.3	236
8	Dynamics of land use/cover changes and the analysis of landscape fragmentation in Dhaka Metropolitan, Bangladesh. Geo Journal, 2012, 77, 315-330.	1.7	189
9	Scaling of land surface temperature using satellite data: A case examination on ASTER and MODIS products over a heterogeneous terrain area. Remote Sensing of Environment, 2006, 105, 115-128.	4.6	186
10	Lunar Radar Sounder Observations of Subsurface Layers Under the Nearside Maria of the Moon. Science, 2009, 323, 909-912.	6.0	166
11	A case study on the relation between city planning and urban growth using remote sensing and spatial metrics. Landscape and Urban Planning, 2011, 100, 223-230.	3.4	136
12	The Ganges and Brahmaputra rivers in Bangladesh: basin denudation and sedimentation. Hydrological Processes, 1999, 13, 2907-2923.	1.1	127
13	Estimation of storage heat flux in an urban area using ASTER data. Remote Sensing of Environment, 2007, 110, 1-17.	4.6	126
14	An automated approach for updating land cover maps based on integrated change detection and classification methods. ISPRS Journal of Photogrammetry and Remote Sensing, 2012, 71, 86-95.	4.9	113
15	Spectral indices for lithologic discrimination and mapping by using the ASTER SWIR bands. International Journal of Remote Sensing, 2003, 24, 4311-4323.	1.3	110
16	Long-term trends and spatial patterns of satellite-retrieved PM2.5 concentrations in South and Southeast Asia from 1999 to 2014. Science of the Total Environment, 2018, 615, 177-186.	3.9	100
17	ASTER instrument characterization and operation scenario. Advances in Space Research, 1999, 23, 1415-1424.	1.2	79
18	Distinguishing the vegetation dynamics induced by anthropogenic factors using vegetation optical depth and AVHRR NDVI: A cross-border study on the Mongolian Plateau. Science of the Total Environment, 2018, 616-617, 730-743.	3.9	73

#	Article	IF	CITATIONS
19	Suspended sediment in the Ganges and Brahmaputra Rivers in Bangladesh: observation from TM and AVHRR data. Hydrological Processes, 2001, 15, 493-509.	1.1	64
20	A high-resolution and multi-year emissions inventory for biomass burning in Southeast Asia during 2001–2010. Atmospheric Environment, 2014, 98, 8-16.	1.9	63
21	Comparison of global inventories of CO2 emissions from biomass burning during 2002–2011 derived from multiple satellite products. Environmental Pollution, 2015, 206, 479-487.	3.7	62
22	Twenty Years of ASTER Contributions to Lithologic Mapping and Mineral Exploration. Remote Sensing, 2019, 11, 1394.	1.8	61
23	A Combination of TsHARP and Thin Plate Spline Interpolation for Spatial Sharpening of Thermal Imagery. Remote Sensing, 2014, 6, 2845-2863.	1.8	57
24	Simulating terrestrial carbon fluxes using the new biosphere model "biosphere model integrating eco-physiological and mechanistic approaches using satellite data―(BEAMS). Journal of Geophysical Research, 2005, 110, n/a-n/a.	3.3	54
25	Instrumentation and observation target of the Lunar Radar Sounder (LRS) experiment on-board the SELENE spacecraft. Earth, Planets and Space, 2008, 60, 321-332.	0.9	53
26	The Lunar Radar Sounder (LRS) Onboard theÂKAGUYA (SELENE) Spacecraft. Space Science Reviews, 2010, 154, 145-192.	3.7	50
27	Preflight and In-Flight Calibration Plan for ASTER. Journal of Atmospheric and Oceanic Technology, 1996, 13, 321-335.	0.5	49
28	Urban growth and change analysis using remote sensing and spatial metrics from 1975 to 2003 for Hanoi, Vietnam. International Journal of Remote Sensing, 2011, 32, 1901-1915.	1.3	47
29	Spatio-temporal evaluation of carbon emissions from biomass burning in Southeast Asia during the period 2001–2010. Ecological Modelling, 2014, 272, 98-115.	1.2	44
30	Long-term trends and spatial patterns of PM2.5-induced premature mortality in South and Southeast Asia from 1999 to 2014. Science of the Total Environment, 2018, 631-632, 1504-1514.	3.9	42
31	Satellite-derived mineral mapping and monitoring of weathering, deposition and erosion. Scientific Reports, 2016, 6, 23702.	1.6	41
32	Comparing terrestrial carbon fluxes from the scale of a flux tower to the global scale. Ecological Modelling, 2007, 208, 135-144.	1.2	40
33	Satellite-driven estimation of terrestrial carbon flux over Far East Asia with 1-km grid resolution. Remote Sensing of Environment, 2011, 115, 1758-1771.	4.6	40
34	Distribution of suspended sediment in the coastal sea off the Ganges–Brahmaputra River mouth: observation from TM data. Journal of Marine Systems, 2002, 32, 307-321.	0.9	37
35	Mechanism of caldera collapse and resurgence: Observations from the northern part of the Kumano Acidic Rocks, Kii peninsula, southwest Japan. Journal of Volcanology and Geothermal Research, 2007, 167, 263-281.	0.8	36
36	High-Resolution Mapping of Biomass Burning Emissions in Three Tropical Regions. Environmental Science & Technology, 2015, 49, 10806-10814.	4.6	36

#	Article	IF	CITATIONS
37	Detection of a landslide movement as geometric misregistration in image matching of SPOT HRV data of two different dates. International Journal of Remote Sensing, 2003, 24, 3523-3534.	1.3	33
38	Fe-oxide concretions formed by interacting carbonate and acidic waters on Earth and Mars. Science Advances, 2018, 4, eaau0872.	4.7	33
39	Aster early image evaluation. Advances in Space Research, 2001, 28, 69-76.	1.2	31
40	Distribution of the subsurface reflectors of the western nearside maria observed from Kaguya with Lunar Radar Sounder. Geophysical Research Letters, 2009, 36, .	1.5	31
41	Characterization and evaluation of MODIS-derived Drought Severity Index (DSI) for monitoring the 2009/2010 drought over southwestern China. Natural Hazards, 2014, 74, 2129-2145.	1.6	31
42	Reducing the Discrepancy Between ASTER and MODIS Land Surface Temperature Products. Sensors, 2007, 7, 3043-3057.	2.1	30
43	Geological mapping of the Francistown area in northeastern Botswana by surface temperature and spectral emissivity information derived from Advanced Spaceborne Thermal Emission and Reflection Radiometer (ASTER) thermal infrared data. Ore Geology Reviews, 2013, 53, 134-144.	1.1	30
44	<title>Scientific basis of ASTER instrument design</title> ., 1993, 1939, 150.		29
45	A multi-year and high-resolution inventory of biomass burning emissions in tropical continents from 2001–2017 based on satellite observations. Journal of Cleaner Production, 2020, 270, 122511.	4.6	29
46	Lunar mare volcanism in the eastern nearside region derived from Clementine UV/VIS data. Meteoritics and Planetary Science, 2003, 38, 1461-1484.	0.7	28
47	Underlying causes of PM2.5-induced premature mortality and potential health benefits of air pollution control in South and Southeast Asia from 1999 to 2014. Environment International, 2018, 121, 814-823.	4.8	28
48	Comparison of global net primary production trends obtained from satellite-based normalized difference vegetation index and carbon cycle model. Global Biogeochemical Cycles, 2001, 15, 351-363.	1.9	27
49	Scale Effect of Vegetation-Index-Based Spatial Sharpening for Thermal Imagery: A Simulation Study by ASTER Data. IEEE Geoscience and Remote Sensing Letters, 2012, 9, 549-553.	1.4	27
50	Estimation of the permittivity and porosity of the lunar uppermost basalt layer based on observations of impact craters by SELENE. Journal of Geophysical Research E: Planets, 2013, 118, 1453-1467.	1.5	27
51	Use of Landsat TM/ETM+ to monitor the spatial and temporal extent of spring breakup floods in the Lena River, Siberia. International Journal of Remote Sensing, 2015, 36, 719-733.	1.3	27
52	High-resolution inventory of mercury emissions from biomass burning in tropical continents during 2001–2017. Science of the Total Environment, 2019, 653, 638-648.	3.9	25
53	A comparison of thermal infrared emissivity spectra measured in situ, in the laboratory, and derived from thermal infrared multispectral scanner (TIMS) data in Cuprite, Nevada, U.S.A International Journal of Remote Sensing, 1997, 18, 1571-1581.	1.3	24
54	Estimation of surface iron oxide abundance with suppression of grain size and topography effects. Ore Geology Reviews, 2017, 83, 312-320.	1.1	24

#	Article	IF	CITATIONS
55	Surface Heat Balance Analysis of Tainan City on March 6, 2001 Using ASTER and Formosat-2 Data. Sensors, 2008, 8, 6026-6044.	2.1	23
56	Synthetic Aperture Radar Processing of Kaguya Lunar Radar Sounder Data for Lunar Subsurface Imaging. IEEE Transactions on Geoscience and Remote Sensing, 2012, 50, 2161-2174.	2.7	23
57	Emittance Spectroscopy and Broadband Thermal Remote Sensing Applied to Phosphorite and Its Utility in Geoexploration: A Study in the Parts of Rajasthan, India. Remote Sensing, 2019, 11, 1003.	1.8	22
58	Mineralogical mapping of southern Namibia by application of continuum-removal MSAM method to the HyMap data. International Journal of Remote Sensing, 2013, 34, 5282-5295.	1.3	20
59	Mare volcanism: Reinterpretation based on Kaguya Lunar Radar Sounder data. Journal of Geophysical Research E: Planets, 2014, 119, 1037-1045.	1.5	17
60	Monitoring the dynamics of ice shelf margins in Polar Regions with high-spatial- and high-temporal-resolution space-borne optical imagery. Cold Regions Science and Technology, 2009, 55, 14-22.	1.6	16
61	Vegetation, water and thermal stress index for study of drought in Nepal and central northeastern India. International Journal of Remote Sensing, 2010, 31, 903-912.	1.3	16
62	Assessing the Impacts of the 2009/2010 Drought on Vegetation Indices, Normalized Difference Water Index, and Land Surface Temperature in Southwestern China. Advances in Meteorology, 2017, 2017, 1-9.	0.6	16
63	Image-scale and look-direction effects on the detectability of lineaments in radar images. Remote Sensing of Environment, 1985, 17, 117-127.	4.6	15
64	Estimation of snow ablation under a dust layer covering a wide range of albedo. Hydrological Processes, 2002, 16, 2853-2865.	1.1	15
65	High-resolution and multi-year estimation of emissions from open biomass burning in Northeast China during 2001–2017. Journal of Cleaner Production, 2021, 310, 127496.	4.6	15
66	Observation and estimation of daily actual evapotranspiration and evaporation on a glacierized watershed at the headwater of the Urumqi River, Tianshan, China. Hydrological Processes, 1999, 13, 1589-1601.	1.1	14
67	Discrepancy Between ASTER- and MODIS- Derived Land Surface Temperatures: Terrain Effects. Sensors, 2009, 9, 1054-1066.	2.1	14
68	Magma source transition of lunar mare volcanism at 2.3ÂGa. Meteoritics and Planetary Science, 2017, 52, 1899-1915.	0.7	14
69	Multi-temporal analysis of deforestation in Rondônia state in Brazil using Landsat MSS, TM, ETM+ and NOAA AVHRR imagery and its relationship to changes in the local hydrological environment. International Journal of Remote Sensing, 2003, 24, 4467-4479.	1.3	13
70	Assessment of values and trends in coarse spatial resolution NDVI datasets in Southeast Asia landscapes. European Journal of Remote Sensing, 2018, 51, 863-877.	1.7	13
71	Integration and Visualization of Mineralogical and Topographical Information Derived from ASTER and DEM Data. Remote Sensing, 2019, 11, 162.	1.8	13
72	An approach to estimating evapotranspiration in the Urumqi River basin, Tianshan, China, by means of remote sensing and a geographical information system technique. Hydrological Processes, 2005, 19, 1839-1854.	1.1	12

#	Article	IF	CITATIONS
73	Temporal influences on Landsatâ€5 Thematic Mapper image in visible band. International Journal of Remote Sensing, 2006, 27, 3183-3201.	1.3	12
74	Quantifying the spatial differences of landscape change in the Hai River Basin, China, in the 1990s. International Journal of Remote Sensing, 2012, 33, 4482-4501.	1.3	12
75	ENSO- and Rainfall-Sensitive Vegetation Regions in Indonesia as Identified from Multi-Sensor Remote Sensing Data. ISPRS International Journal of Geo-Information, 2018, 7, 103.	1.4	12
76	A monthly stream flow model for estimating the potential changes of river runoff on the projected global warming. Hydrological Processes, 2000, 14, 1851-1868.	1.1	10
77	Scientific exploration of lunar surface using a rover in Japanese future lunar mission. Advances in Space Research, 2002, 30, 1921-1926.	1.2	10
78	ASTER views a high altitude Tibetan Lake in stereo. Eos, 2004, 85, 435.	0.1	10
79	Scientific results from ASTER. Remote Sensing of Environment, 2005, 99, 1.	4.6	10
80	An Automated Method for Crater Counting Using Rotational Pixel Swapping Method. IEEE Transactions on Geoscience and Remote Sensing, 2017, 55, 4384-4397.	2.7	10
81	Possible techniques for lithologic discrimination using the short-wavelength-infrared bands of the Japanese ERS-1. Remote Sensing of Environment, 1987, 23, 117-129.	4.6	9
82	Delineation of small-scale landforms relative to flood inundation in the western Red River delta, northern Vietnam using remotely sensed data. Natural Hazards, 2013, 69, 905-917.	1.6	8
83	Evaluation of the Effect of Preâ€processing of the Remotely Sensed Data on the Actual Evapotranspiration, Surface Soil Moisture Mapping by an Approach Using Landsat, DEM and Meteorological Data. Geocarto International, 2000, 15, 59-70.	1.7	7
84	Comparison of surface heat balance in three cities in Taiwan using Terra ASTER and Formosat-2 RSI data. International Journal of Applied Earth Observation and Geoinformation, 2012, 18, 263-273.	1.4	7
85	Climate-Induced Extreme Hydrologic Events in the Arctic. Remote Sensing, 2016, 8, 971.	1.8	7
86	A simple global carbon and energy coupled cycle model for global warming simulation: sensitivity to the light saturation effect. Tellus, Series B: Chemical and Physical Meteorology, 2003, 55, 676-691.	0.8	6
87	First space-borne high-spatial-resolution optical imagery of the Antarctic from Formosat-2. Antarctic Science, 2008, 20, 605-606.	0.5	6
88	Effects of topography on the spatial distribution of evapotranspiration over a complex terrain using twoâ€source energy balance model with ASTER data. Hydrological Processes, 2009, 23, 2295-2306.	1.1	6
89	A new one-dimensional simple energy balance and carbon cycle coupled model for global warming simulation. Theoretical and Applied Climatology, 2010, 101, 459-473.	1.3	6
90	The layered structure of lunar maria: Identification of the HF-radar reflector in Mare Serenitatis using multiband optical images. Icarus, 2012, 218, 506-512.	1.1	6

#	Article	IF	CITATIONS
91	Rotational Pixel Swapping Method for Detection of Circular Features in Binary Images. IEEE Transactions on Geoscience and Remote Sensing, 2015, 53, 710-723.	2.7	5
92	Retrieval algorithms for photopolarimetric properties of aerosols. Advances in Space Research, 1996, 17, 63-66.	1.2	4
93	Quantifying variability of satellite data in the reflective band for long-term monitoring of the Earth's surface: inference from a multi-temporal relationship between remotely sensed pixels. International Journal of Remote Sensing, 2011, 32, 7717-7730.	1.3	4
94	Weighted misclassification rate: a new measure of classification error designed for landscape pattern index. Remote Sensing Letters, 2012, 3, 57-65.	0.6	4
95	Identification of Alteration Minerals from Unstable Reflectance Spectra Using a Deep Learning Method. Geosciences (Switzerland), 2019, 9, 195.	1.0	4
96	GEOLOGICAL MAPPING BY COMBINING SPECTRAL UNMIXING AND CLUSTER ANALYSIS FOR HYPERSPECTRAL DATA. International Archives of the Photogrammetry, Remote Sensing and Spatial Information Sciences - ISPRS Archives, 0, XLI-B8, 431-435.	0.2	4
97	Characterizing the Urban Growth of Hanoi, Nagoya, and Shanghai City using Remote Sensing and Spatial Metrics. , 2008, , .		3
98	Relative Importance of Climatic and Anthropogenic Drivers on the Dynamics of Aboveground Biomass across Agro-Ecological Zones on the Mongolian Plateau. Sustainability, 2018, 10, 3435.	1.6	3
99	Reflectances in the Ganges and Brahmaputra rivers and in the adjacent coastal sea. International Journal of Remote Sensing, 2000, 21, 2213-2224.	1.3	2
100	A new approach to reduce inconsistency between MODIS and ASTER land surface temperature products. , 2006, , .		2
101	Analysis of deforestation in Mato Grosso using multi-temporal Landsat TM Imageries. , 2010, , .		2
102	Soft image segmentation model. , 2012, , .		2
103	The Lunar Radar Sounder (LRS) Onboard the Kaguya (SELENE) Spacecraft. , 2010, , 145-192.		2
104	<title>Japanese mission overview of JERS and ASTER programs</title> ., 1991, , .		1
105	Current status and science objectives of ASTER project. Advances in Space Research, 1994, 14, 141-145.	1.2	1
106	In-flight test site calibration of EOS-AM1/ASTER/TIR with MODIS. Advances in Space Research, 1994, 14, 227-230.	1.2	1
107	<title>ASTER early science outcome and operation status</title> ., 2001, , .		1
108	A simple global carbon and energy coupled cycle model for global warming simulation: sensitivity to the light saturation effect. Tellus, Series B: Chemical and Physical Meteorology, 2003, 55, 676-691.	0.8	1

#	Article	IF	CITATIONS
109	ASTER science outcome and operation status. , 0, , .		1
110	Automated micro-landform classification by combination of satellite images and SRTM DEM. , 2011, , .		1
111	Scale effect of vegetation index based thermal sharpening: A simulation study based on aster data. , 2011, , .		1
112	Evolution of NASA's Earth Observing System and Development of the Moderate-Resolution Imaging Spectroradiometer and the Advanced Spaceborne Thermal Emission and Reflection Radiometer Instruments. Remote Sensing and Digital Image Processing, 2010, , 3-34.	0.7	1
113	<title>ASTER target observation scenario</title> ., 2001, 4169, 67.		0
114	<title>Overview of ASTER instrument and ASTER data product</title> ., 2002, , .		0
115	Studies on Surface Temperature using Remote Sensing Technique in the NW Part of Bangladesh. Geocarto International, 2003, 18, 41-49.	1.7	0
116	Error analysis of scaling evapotranspiration over heterogeneous land surface. , 2006, , .		0
117	An advanced method for mineral mapping applicable to hyperspectral images: the composite MSAM. Remote Sensing Letters, 2015, 6, 499-508.	0.6	0
118	Monitoring Spring Floods on the Lena River Using Multiple Satellite Sensors. Global Environmental Studies, 2018, , 53-69.	0.2	0
119	Editorial for the Special Issue "ASTER 20th Anniversary― Remote Sensing, 2020, 12, 884.	1.8	0
120	The New Version 3 Aster Global DEM and the Aster Water Body Dataset. , 2021, , .		0
121	ASTER Application in Urban Heat Balance Analysis: A Case Study of Nagoya. Remote Sensing and Digital Image Processing, 2010, , 375-395.	0.7	0